# Commensurate-incommensurate transitions in quantum films: Submonolayer molecular hydrogen on graphite

Kwangsik Nho
*Center for Simulational Physics, University of Georgia, Athens, Georgia 30602-2451*

Efstratios Manousakis
*Department of Physics and MARTECH, Florida State University, Tallahassee, Florida 32306*
*and Department of Physics, University of Athens, Panepistimiopolis, Zografos, 157 84 Athens, Greece*
(Received 27 December 2002; published 27 May 2003)

We have used the path-integral Monte Carlo method to simulate a monolayer of molecular hydrogen on graphite above 1/3 submonolayer coverage. We find that at low temperature and as the coverage increases, the system undergoes a series of transformations starting from the $\sqrt{3}\times\sqrt{3}$ commensurate solid near 1/3 coverage. First, a phase is formed, which is characterized by a uniaxially compressed incommensurate solid with additional mass density modulations along the same direction, which can be viewed as an ordered domain-wall solid with a characteristic domain-wall distance that depends on the surface coverage. At low temperature and higher coverage there is a transition to an incommensurate solid, which is rotated relative to the substrate commensurate lattice. As a function of temperature, the domain-wall ordering first melts into a fluid of domain walls and at higher temperature the solid melts into a uniform fluid. Regardless of the large amplitude of quantum fluctuations, these phase transitions are analogous to those in classical monolayer films. Our calculated values for the surface coverage and temperature, where these transitions occur, the calculated structure factors, and specific heat are in general agreement with the available experimental results with no adjustable parameters.

DOI: 10.1103/PhysRevB.67.195411 PACS number(s): 64.60.Fr, 67.40.−w, 67.40.Kh

## I. INTRODUCTION

The commensurate-incommensurate transition has been extensively studied in classical monolayer films both theoretically and experimentally. Monolayers of hydrogen or helium are quantum-mechanical systems and, in principle, one might suspect a different behavior due to the effect of strong quantum fluctuations.

The monolayer phase diagram of molecular parahydrogen adsorbed on graphite as inferred from experimental studies[1] is shown in Fig. 1. This phase diagram was originally drawn based on the anomalies found in the specific heat;[2–4] for the characterization of the various phases, low-energy electron-diffraction[5–7] (LEED) as well as neutron-diffraction[1,8,9] studies have been carried out. At 1/3 coverage the molecules condense on the surface of graphite in a $\sqrt{3}\times\sqrt{3}$ commensurate solid. In the low coverage region ($\rho<0.6$) (in units of the $\sqrt{3}\times\sqrt{3}$ commensurate density), it forms a commensurate solid-gas coexistence phase at low temperature and a two-dimensional (2D) gas phase at higher temperature ($T>10$ K). For coverages $0.6\lesssim\rho\lesssim0.9$, as a function of temperature, there is a transition from a commensurate solid cluster phase to a commensurate solid phase with vacancies at higher temperature and to a 2D gas at even higher temperature. At density somewhat higher than unity, the so-called $\alpha$ phase is formed, which is believed to be a striped domain-wall solid phase and at higher temperature it transforms to the so-called $\beta$ phase and to a fluid phase at even higher temperature. At high densities a transition take place to a triangular incommensurate solid phase.

The phase diagram of molecules formed from the isotopes of hydrogen such $D_2$ and HD molecules physiorbed on graphite has also been studied[10,11] and it is similar to that of $H_2$ on graphite but is more complex.

We have recently studied[12] the phase diagram of molecular hydrogen on graphite at and below 1/3 coverage using path-integral Monte Carlo (PIMC) simulation. Our computed phase diagram was, in general, agreement with that inferred from the experimental studies for this coverage range. In this paper we extend the PIMC calculation to study the phase diagram above the commensurate density, which is less well understood both theoretically and experimentally. At coverages above $\rho\simeq1.05$, the monolayer undergoes a commensurate-incommensurate(C-IC) transition. While the existence of the so-called $\alpha$ and $\beta$ phases was known from the specific-heat anomalies, their characterization came from LEED (Refs. 6,7) and neutron-scattering[1] studies. Using LEED experiments, Cui and Fain[6,7] observed a uniaxial IC solid with striped superheavy domain walls and a rotated triangular IC solid at higher coverages $\rho\geqslant1.23$. Freimuth, Wiechert, and Lauter[1] (FWL) presented a neutron-diffraction study of the C-IC transition and their results are in agreement with the LEED results. They examined the commensurate-incommensurate solid transition, especially the striped domain-wall solid phase. In the $\alpha$ phase the diffraction intensity has a main peak characteristic of a compressed lattice and a satellite peak on the lower side of the commensurate peak wave-vector position $k_c=1.703$ Å$^{-1}$ that arise from the spatial modulation due to ordered striped domain walls. As coverage increases, the separation of the two peaks increases and the satellite intensity decreases. At higher temperatures the peak height drops and the satellite peak vanishes which

 

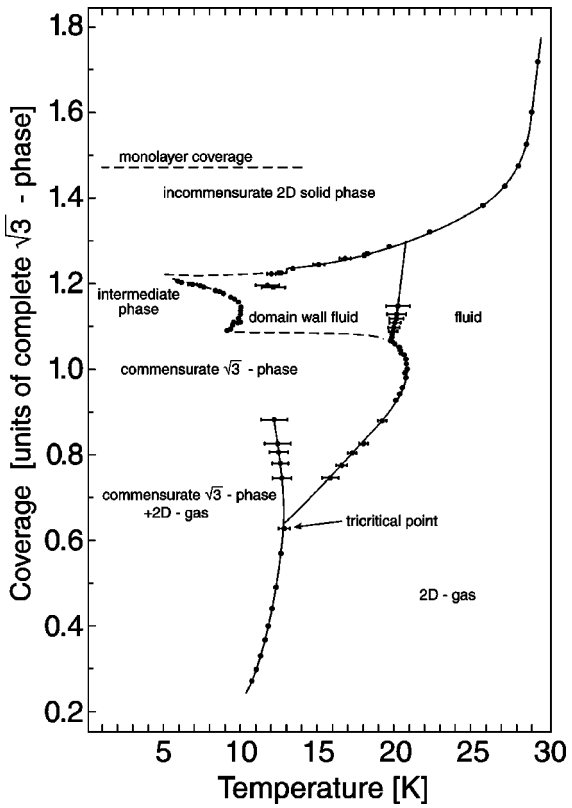


FIG. 1. Phase diagram of molecular hydrogen adsorbed on graphite from Ref. 9 (reproduced here for easy reference). Density 1.0 corresponds to the complete commensurate $\sqrt{3}\times\sqrt{3}$ phase.

implies that the commensurate domains vanish and the system becomes an isotropic fluid phase. As coverage increases, the first molecular hydrogen layer forms a rotated incommensurate solid phase. Neutron-diffraction studies show a sharp and intense peak at wave vector $k=1.97$ Å$^{-1}$ at the density $\rho=1.34$, which reveals an IC equilateral triangular structure. This phase is continuously compressed, as the coverage increases up to the highest density allowed before layer promotion.

In parallel to these experimental investigations, several important theoretical studies were undertaken to understand the commensurate-incommensurate transition[13–17] in physiorbed systems. The phases and the phase transitions that were theoretically predicted and studied can be understood as classical phenomena due to the strain induced on the adsorbate molecules of the monolayer film due to the substrate periodic structure which arise from the competition between adsorbate-adsorbate and adsorbate-substrate interactions. Molecular hydrogen and atomic helium physiorbed on graphite are quantum films characterized by strong zero-point motion. Therefore, one can find out the degree to which a classical picture might be valid and might expect new phenomena and phases to occur. Motivated by these thoughts, we extended our earlier investigation[12] to study this system above 1/3 coverage up to layer completion starting from the known hydrogen molecule-molecule and hydrogen-graphite interactions[20–23] and using the PIMC,[19] which is a Quantum Monte Carlo technique adopted for the study of strongly interacting quantum films by Pierce and Manousakis.[18]

We have simulated the first layer of molecular hydrogen on graphite with a variety of simulation cells that are appropriate for examining different phase regions of the phase diagram. We have applied periodic boundary conditions along both directions parallel to the surface of the substrate. We have computed expectation values for the total energy, the static structure factor, the probability distribution, and the specific heat by means of the path-integral Monte Carlo (MC) simulation method using the multilevel Metropolis method. In the multilevel bisection method we have used level 3 that optimizes the acceptance ratio. To thermalize the system, we typically carried out of the order of 15 000 MC steps, and we carried out of the order of 2000–20 000 MC steps in order to compute observables.

## II. UNIAXIALLY COMPRESSED SOLID WITH ORDERED DOMAIN WALLS

In this section we discuss the region above the commensurate coverage where experimentally the ordered domain-wall solid was found. We carried out a simulation at two densities in this region, the same densities discussed by FWL, where they inferred the existence of relaxed superheavy domain walls.

We used simulation cells that can accommodate the structures that have been proposed by FWL.

(a) First, we consider $\rho=0.0694$ Å$^{-2}$. We have chosen a simulation cell with dimensions $x=5\sqrt{3}a_{gr}$ and $y=22a_{gr}$, where $a_{gr}=2.459$ Å is the carbon-carbon distance on the graphite surface and 80 hydrogen molecules to produce the above density. In Fig. 2 we give the contour plot of the calculated probability distribution where we see that two commensurate-solid domains are separated by the incommensurate solid domains. The solid structure is uniaxially compressed along our $y$ direction such that a new row of molecules is introduced every eight rows. Notice that the period in the $x$ direction is $\sqrt{3}a_{gr}$ and there is modulation along the $y$ direction with period $11a_{gr}$, so that the wavelength $\lambda_s$ of this striped domain-wall modulation is $\lambda_s=27.049$.

(b) Second, we have performed the simulation at density $\rho=0.0716$ Å$^{-2}$. We have chosen a simulation cell with dimensions $x=5\sqrt{3}a_{gr}$ and $y=16a_{gr}$ and 60 hydrogen molecules in order to achieve the above-mentioned density. The calculated contour plot of the probability distribution is shown in Fig. 3. Notice that, in this case also, there is an ordered striped domain-wall solid phase along our $y$ direction; namely, the amplitude of the molecular density wave is modulated along the $y$ axis with a period of about half our cell size along the $y$ axis. Notice that there are two commensurate solid domains separated by denser regions.

Our computed static structure factor $S(k)$ for $\rho=0.0694$ Å$^{-2}$ is shown in Fig. 4. The main Bragg peaks of this structure occur at $\mathbf{k}_1=(1.475\ \text{Å}^{-1},0.929\ \text{Å}^{-1})$ and $\mathbf{k}_2=(0,1.858\ \text{Å}^{-1})$. The satellite peak occurs at $\mathbf{k}_{sat}^{c}=(0,1.626\ \text{Å}^{-1})$. The experimental values of the magnitudes of the wave vectors at the peaks are $k_{main}^{exp}=1.743$ Å$^{-1}$ and $k_{sat}^{exp}=1.632$ Å$^{-1}$, which compare well

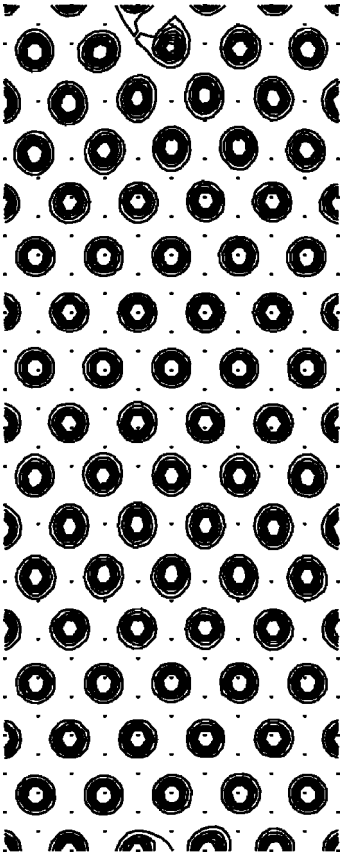

FIG. 2. Contour plot of the probability distribution at the density 0.0694 Å$^{-2}$ and $T=1.33$ K. The simulation cell is 21.295 Å $\times$54.098 Å (80 $H_2$ molecules). The filled circles indicate graphite adsorption sites. The solid structure is uniaxially compressed along our $y$ direction. In addition, two commensurate solid domains separated by the incommensurate solid domains can be seen, which implies a mass density wave along the same direction.

with our computed values of $k_1^c=1.743$ Å$^{-1}$ and $k_{sat}^c=1.626$ Å$^{-1}$. We believe that FWL could not observe the peak at $\mathbf{k}_2$ because of the strong interference with the (002) graphite peak.

The interpretation of these results is as follows. Analyzing the contour plot of Fig. 2 we find that (a) the solid appears uniaxially compressed along the $y$ direction, by adding another row for every ten rows of molecules and spreading them evenly, while along the $x$ direction the average spacing between the molecules remains that of the commensurate solid. (b) Superimposed there is a density modulation along the $y$ direction, which has wavelength several times greater than the average nearest-neighbor distance but of small amplitude. The actual size of the wavelength $\lambda_s$ of this striped domain-wall modulation is half of the length of our simulation cell in the $y$ direction, i.e., $\lambda_s=27.05$ Å, as discussed above. The two main Bragg peaks correspond to the unit vectors that span the reciprocal space of this uniaxially compressed triangular solid structure. The satellite peaks are due to lateral modulation in our $y$ direction and are located at $\mathbf{k}_{sat}=\mathbf{k}_{1,2}-\mathbf{k}_s$ . $\mathbf{k}_{1,2}$ correspond to the wave vector of each of the two main Bragg peaks and $\mathbf{k}_s=(0,2\pi/\lambda_s)$, where $\lambda_s$ is the wavelength of a unit cell for the striped domain-wall

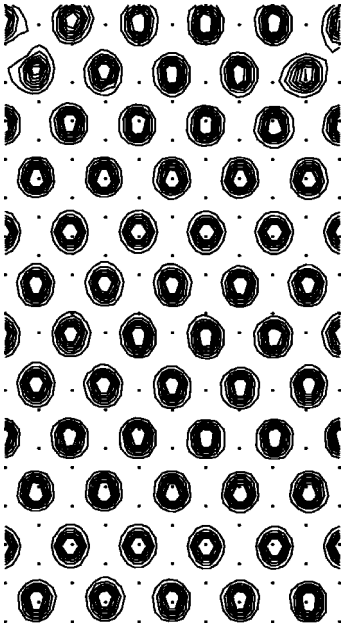

FIG. 3. Contour plot of the probability distribution at density 0.0716 Å$^{-2}$ for $T=1.33$ K. The simulation cell is 21.295 Å $\times$39.344 Å (60 molecules). The filled circles indicate graphite adsorption sites. The solid structure is uniaxially compressed along our $y$ direction. The striped domain-wall solid phase can be seen.

solid structure in the modulated direction. Using this $\lambda_s$ value, $\mathbf{k}_2=(0,1.858$ Å$^{-1})$ and $\mathbf{k}_s=(0,0.232$ Å$^{-1})$ (obtained by using the values of $\lambda_s=27.049$ Å found by inspection of Fig. 2), we can find that the satellite peak position is at $\mathbf{k}_{sat}=(0,1.626$ Å$^{-1})$, which agrees well with our peak value.

The structure factor for the case of $\rho=0.0716$ Å$^{-2}$ (Fig. 3) is shown in Fig. 5. The main peaks are $\mathbf{k}_1=(1.475$ Å$^{-1}$,0.958 Å$^{-1})$ and $\mathbf{k}_2=(0,1.916$ Å$^{-1})$, which correspond to the uniaxially compressed solid produced by

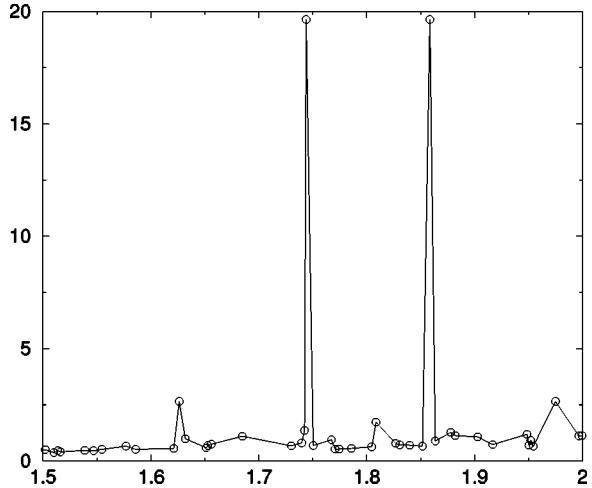


FIG. 4. Static structure factor $S(k)$ at density 0.0694 Å$^{-2}$ (and corresponds to Fig. 2) for $T=1.33$ K as a function of the magnitude of $\vec{k}$. The main Bragg peaks are at $k_1=1.743$ Å$^{-1}$ and $k_2=1.858$ Å$^{-1}$. There is a satellite peak located at $k_{sat}^c=1.626$ Å$^{-1}$.

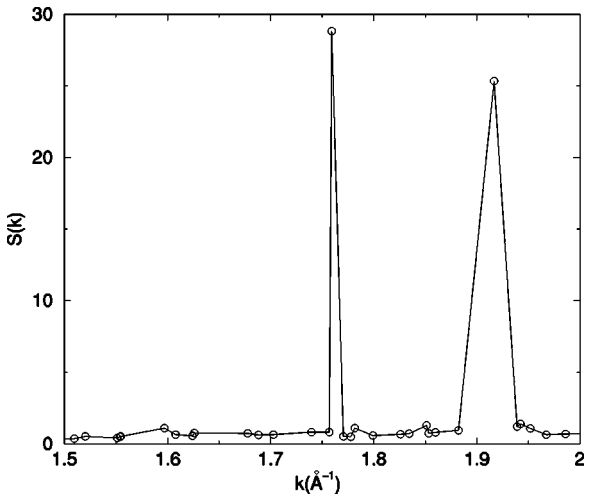


FIG. 5. Static structure factor $S(k)$ at the density 0.0716 Å$^{-2}$ (and corresponds to Fig. 3) for $T=1.33$ K. The main Bragg peaks are at $k_1=1.759$ Å$^{-1}$ and $k_2=1.916$ Å$^{-1}$. Notice that the satellite peak at $k_{sat}^c=1.597$ Å$^{-1}$ is significantly weaker than the satellite peak at the lower density shown in Fig. 4.

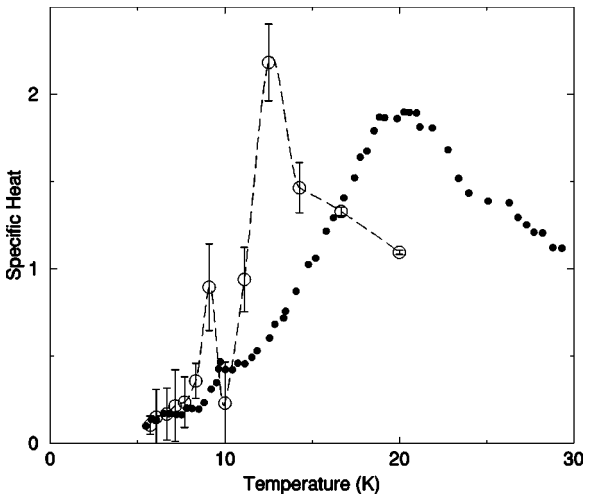


FIG. 7. Specific heat versus temperature at density 0.0716 Å$^{-2}$. The long-dashed line is a spline fit to the specific-heat values and is a guide to the eye. The filled circles are the experimental specific heat at the density 0.0716 Å$^{-2}$. The simulation cell is 29.813 Å $\times$39.344 Å (84 $H_2$ molecules). Our computed values for the melting and evaporation temperature are the peak positions, 9.09 K and 12.5 K, respectively.

adding another row of molecules for every six rows of molecules and spreading them evenly. This, in addition, forms a superstructure with wavelength $\lambda_s=19.672$ Å which gives a satellite peak at $\mathbf{k}_{sat}^c=(0,1.597\ \text{Å}^{-1})$. Notice that the scattering intensity, relative to the previously discussed case of $\rho=0.0694$ Å$^{-2}$, has the peaks shifted at higher values of $k$ as expected and the intensity of the satellite peaks is decreased as in the experiments.

### III. DOMAIN-WALL MELTING

In Fig. 6 we show the contour plot of the the probability distribution where a striped domain-wall fluid phase (at $T=11.11$ K) and a fluid phase (at $T=16.67$) are evident. Notice that the stripe domain-wall fluid phase (left part of Fig. 6) is characterized by mobile commensurate and incommensurate domains. To understand this contour plot, we need to be reminded of the periodic boundary conditions used in our simulation and the fact that these domains cannot intersect each other. This implies that one domain will oscillate back and forth between the neighboring domains.

We would like to call the reader's attention to the presence of strong finite-size effects in this study of the domain-wall melting. In addition, the domain boundary melting is analogous to the roughening of vicinal surfaces and meandering of steps, and our simulation cell is not wide enough to encompass formation of kink pairs along the domain boundaries. We can very approximately determine the melting temperature of the domain-wall solid phase from the temperature dependence of the specific heat and from the temperature dependence of the peak height of the static structure factor $S(k)$.

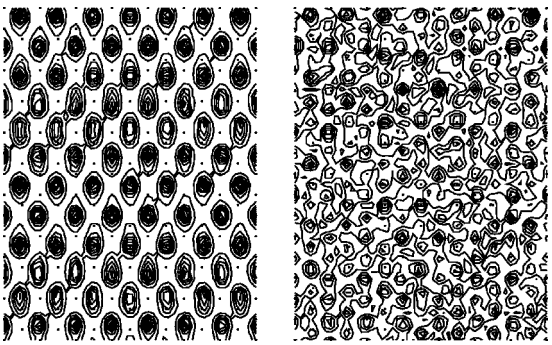

FIG. 6. Contour plot of the probability distribution at density 0.0716 Å$^{-2}$ at two temperatures 11.11 K and 16.67 K.

The calculated specific heat as a function of temperature is shown in Fig. 7 and is characterized by two peaks; the first corresponds to the melting of the domain-wall solid while the second peak indicates the melting of the stripes and the solid into a fluid. Our computed values for the melting temperature are generally lower than the experimental values. For example, for $\rho=0.0716$ Å$^{-2}$ we find that at $T=9.09$ K the striped domain-wall solid phase undergoes a transition to the domain-wall fluid phase and at $T=12.5$ K the $\beta$ phase becomes an isotropic fluid phase. Factors for obtaining lower values for the critical temperature than the experimental values could be the finite-size effects and the interaction strength used to describe the hydrogen-graphite interaction. We also computed the static structure factor shown in Fig. 8 and we studied the temperature dependence of the height of its first main peak, which is shown in Fig. 9. The peak height significantly decreases near the melting temperature of the domain-wall solid and near the domain-wall evaporation temperature.

Clearly much larger size lattices are needed to study the nature of this phase transition. Such a study is beyond our current computational resources and we restrict ourselves to our qualitative results obtained here with full quantum-mechanical treatment of the problem. In a different line of

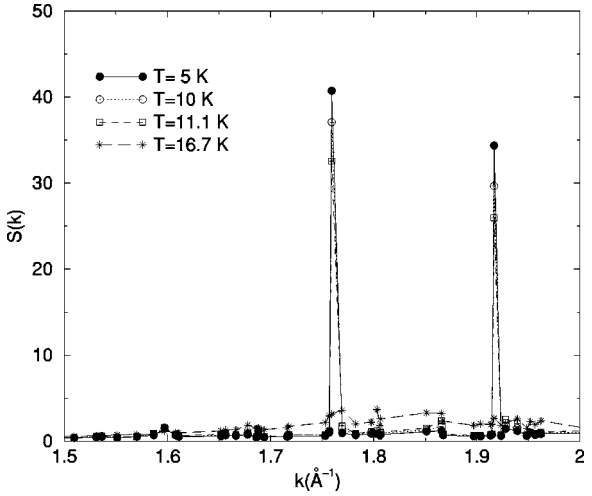


FIG. 8. Static structure factor $S(k)$ at the density 0.0716 Å$^{-2}$ for various temperatures.

work, one can use classical simulations of models of such stripe melting to carefully examine finite-size effects.

## IV. ROTATED INCOMMENSURATE SOLID

The first layer of molecular hydrogen adsorbed on graphite forms an incommensurate solid phase before the first layer is complete. We have carried out a simulation at density $\rho = 0.0849$ Å$^{-2}$ using a simulation cell with dimensions $x = 9\sqrt{3}a_{gr}$ and $y = 9a_{gr}$. The calculated probability distribution (Fig. 10) also clearly shows the presence of an equilateral triangular solid structure, which is not registered with the underlying graphite lattice and it is rotated relative to the graphite lattice. This rotation was first predicted and discussed by Novaco and McTague.[13] The angle of the incommensurate lattice relative to the graphite lattice is approximately 5°, in good agreement with the experimental value[7] for the above density. The calculated static structure factor (shown in Fig. 11) has one sharp peak at $k = 1.99$ Å$^{-1}$ corresponding to an unregistered equilateral triangular lattice in agreement with the value of $k = 1.97$ Å$^{-1}$ reported from the neutron-diffraction experimental study.[1]

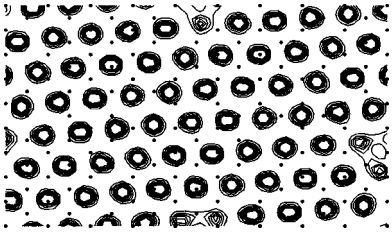

FIG. 10. Contour plot of the probability distribution at density 0.0849 Å$^{-2}$. The simulation cell is 38.331 Å$\times$22.131 Å (72 $H_2$ molecules).

## V. ENERGY CALCULATION

In Fig. 12 we compare the energy per hydrogen molecule as a function of the surface coverage for the cases where the full potential is used (solid line) and the case where only the laterally averaged potential is used (dashed line). There are several important observations that we will make based on the results presented in this figure. First the curve obtained using the laterally averaged potential has a minimum at density $\rho_0 = 0.0705$ Å$^{-2}$. At this equilibrium density the system forms a triangular lattice that fills the entire system and below this density the system undergoes a phase separation and forms a solid-vapor coexistence phase. Therefore below $\rho_0$ the energy as a function of density is higher for a finite-size system or for a system that is forced to be uniform at this lower density. Above this density the system is a compressed triangular solid until the promotion density.[12] The solid line corresponds to the energy per molecule when we used the hydrogen-molecule-graphite interaction potential with the corrugations. The minimum in this case occurs at $\rho_c = 0.0636$ Å$^{-2}$, which corresponds to the $\sqrt{3}\times\sqrt{3}$ solid. Below that density, the system is unstable to formation of solid

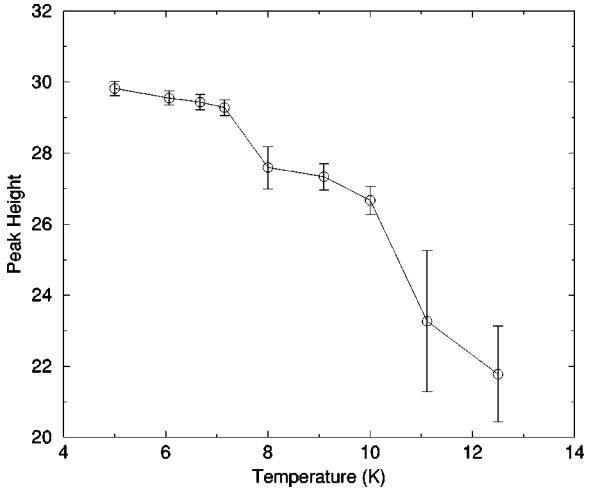


FIG. 9. The peak height of the static structure factor $S(k)$ versus temperature at the density 0.0716 Å$^{-2}$. The simulation cell is 21.295 Å$\times$39.344 Å (60 molecules).

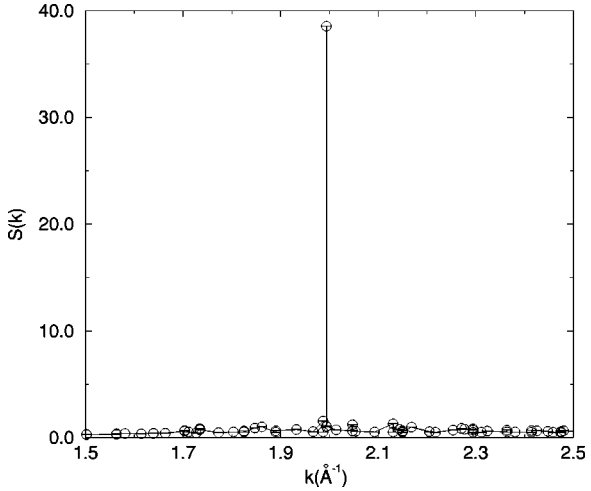


FIG. 11. Static structure factor $S(k)$ at density 0.0849 Å$^{-2}$. The simulation cell is 38.331 Å$\times$22.131 Å (72 $H_2$ molecules). The sharp peak position is $k = 1.99$ Å$^{-1}$.

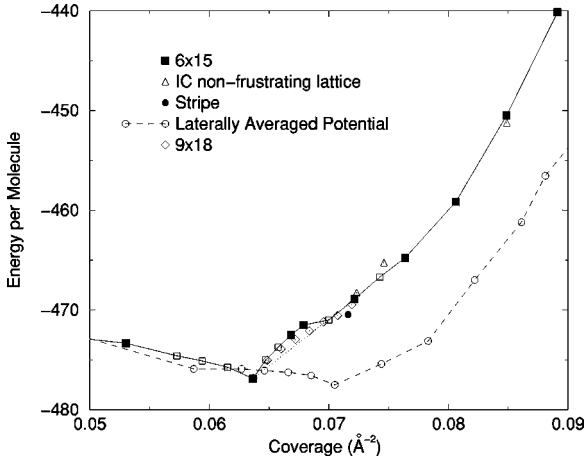


FIG. 12. The dashed line is the energy per hydrogen molecule on the graphite substrate using the laterally averaged potential as a function of surface coverage. The solid line is the same quantity when corrugations are included.

clusters and this part of the phase diagram was investigated in Ref. 12. Above this density, up to a density one can notice that the presence of the substrate corrugations moves the minimum from $\rho_0$ at much higher energy but there is a feature at the same density produced by the $H_2$-$H_2$ interaction. The value $\rho_0$ of the equilibrium density for a smooth substrate plays a significant role even when the full potential with the substrate corrugations is used because it is the density that minimizes the energy due to $H_2$ molecule-molecule interaction. Clearly due to this term, which has a preference for a higher density than the commensurate density, the solid line is not convex that a sign of instability of a uniform phase. These results are obtained on lattices which frustrate the proper periodicity of the domain walls. If the calculations are done on lattices that can accommodate the periodicity of these superlattice structures, the energy is lowered. As an example we also give (solid circle) the energy obtained for the stripe state of Fig. 3. Notice that the energy falls below that obtained with choice of lattices unfavorable for this ordered domain-wall state.

## VI. CONCLUSIONS

Our studies on $H_2$ monolayer on graphite above 1/3 coverage clarifies the nature of the phase diagram. The boundaries of the phase diagram were well known from the specific anomalies. We find that the phase near 1/3 coverage is the known $\sqrt{3}\times\sqrt{3}$ commensurate solid. At higher densities the monolayer undergoes a transition to a uniaxially compressed solid with density wave stripelike modulations along the same direction. This phase was first identified by LEED studies;[6] while the subsequent neutron-diffraction studies[1] confirm the existence of ordered domains walls, the peak that is the signature of the uniaxial compression is not seen because of the (002) reflection from the underlying graphite lattice. In addition in both studies the domain walls are assumed to be superheavy. As is clear from both our contour plots and our structure factor, the walls are not significantly denser than the rest of the system; we find that the additional molecules added to the monolayer to increase the coverage above the commensurate coverage are used primarily to uniaxially compress the solid and they are only partially used to construct the walls. Our calculated specific heat for this coverage range as a function of temperature has two anomalies at two temperature values. From the calculated contour plots and the structure factor, the lower temperature anomaly is identified as the transition from the ordered domain-wall solid to a solid where the domain walls form a fluid and the higher-temperature anomaly is caused by the total melting of the solid to a uniform fluid.

At even higher density we find that the uniaxially compressed solid with the ordered domain walls undergoes a transition to a triangular solid, which is incommensurate with respect to the substrate lattice and, in addition, the triangular solid of the adlayer is rotated by an angle of the order of 5° with respect to the underlying substrate lattice. This is in complete agreement with both the theoretical prediction[13] and experimental findings.[1,6]

## ACKNOWLEDGMENTS

This work was supported by a National Aeronautics and Space Administration Grant No. NAG8-1773.

[1] H. Freimuth, H. Wiechert, and H.J. Lauter, Surf. Sci. **189&190**, 548 (1987).
[2] F.C. Motteler and J.G. Dash, Phys. Rev. B **31**, 346 (1985).
[3] F.A.B. Chaves, M.E.B.P. Cortez, R.E. Rapp, and E. Lerner, Surf. Sci. **150**, 80 (1985).
[4] H. Freimuth and H. Wiechert, Surf. Sci. **162**, 432 (1985).
[5] J.L. Seguin and J. Suzanne, Surf. Sci. **118**, L241 (1982).
[6] J. Cui and S.C. Fain, Jr., Bull. Am. Phys. Soc. **31**, 376 (1986).
[7] J. Cui and S.C. Fain, Jr., Phys. Rev. B **39**, 8628 (1989).
[8] M. Nielsen, J.P. McTague, and W. Ellenson, J. Phys. (Paris), Colloq. **38**, C4-10 (1977); M. Nielsen, J.P. McTague, and L. Passell, in *Phase Transitions in Surface Films*, edited by J.G. Dash and J. Ruvalds (Plenum, New York, 1980).
[9] H. Wiechert, Physica B **169**, 144 (1991).
[10] H. Freimuth, H. Wiechert, H.P. Schildberg, and H.J. Lauter, Phys. Rev. B **42**, 587 (1990).
[11] H.J. Lauter, H. Godfrin, V.L.P. Frank, and P. Leiderer, in *Phase Transitions in Surface Films 2*, edited by H. Taub, G. Torzo, H. J. Lauter, and S.C. Fain, Jr., (Plenum, New York, 1990).
[12] K. Nho and E. Manousakis, Phys. Rev. B **65**, 115409 (2002).
[13] A.D. Novaco and J.P. McTague, Phys. Rev. Lett. **38**, 1286 (1977); J.P. McTague and A.D. Novaco, Phys. Rev. B **19**, 5299 (1979).
[14] J. Villain, Phys. Rev. Lett. **41**, 36 (1978).
[15] P. Bak, D. Mukamel, J. Villain, and K. Wentowska, Phys. Rev. B **19**, 1610 (1979).
[16] S.N. Coppersmith, D.S. Fisher, B.I. Halperin, P.A. Lee, and W.F.

Brinkman, Phys. Rev. Lett. **46**, 549 (1981); Phys. Rev. B **25**, 349 (1982).
[17] T. Halpin-Healy and M. Kardar, Phys. Rev. B **34**, 318 (1986).
[18] M. Pierce and E. Manousakis, Phys. Rev. B **59**, 3802 (1999).
[19] D.M. Ceperley, Rev. Mod. Phys. **67**, 279 (1995).
[20] I.F. Silvera and V.V. Goldman, J. Chem. Phys. **69**, 4209 (1978).
[21] A.D. Crowell and J.S. Brown, Surf. Sci. **123**, 296 (1982).
[22] W.A. Steele, Surf. Sci. **36**, 317 (1973).
[23] W.E. Carlos and M.W. Cole, Surf. Sci. **91**, 339 (1980).